Frequency-Domain Simulation of the Indoor Wireless Optical Communication Channel

Henrik Schulze

The Author is with the South Westphalia University of Applied Sciences, Lindenstr. 53, D-59872 Meschede, Germany. Telephone: (+49) 291 9910-300.
E-mail: schulze@fh-swf.de

***Abstract*—The indoor wireless optical communication channel is characterised by multiple reflections of the light from the surrounding walls. We present a new frequency-domain simulation method for this channel. In contrast to the known time-domain simulation techniques, our method is not restricted to a finite order of reflections. We show that the contributions of an infinite number of reflections can be summed up analytically to a formula that can be handled by standard numerical methods. We illustrate the method by comparing it to results of previous time domain simulations, and we apply it to the numerical evaluation of some further model scenarios with more than one transmitter.**

***Index Terms*—Optical communication, multipath channels, communication channels, channel modelling, channel impulse response.**

I. Introduction

Wireless optical transmission is a promising technology for indoor communication [1], [2] whose potential has not yet been fully exploited. The major benefits of optical transmission are twofold: Firstly, there are no problems with frequency planning as optical signals are not able to go through walls. Secondly, the optical components such as light-emitting diodes (LEDs) in the transmitter and positive intrinsic negative (PIN) photo-diodes in the receiver are not expensive and are easy to handle. This technology uses intensity modulation with direct detection (IM/DD), meaning that the information is conveyed via modulation of the incoherent light intensity, and that the light intensity has to be detected and demodulated by the receiver in order to extract the information.

The indoor reception of an optical signal is affected by multipath propagation of the light that is reflected from the walls and the objects inside the room. The optical multipath channel typically shows a distinct low-pass behaviour [1] that may also include severe notches at certain frequencies due to strong echo components with high runtime differences. Depending on the bandwidth and the modulation scheme of the transmitted signal, the frequency selective behaviour of the optical channel may severely corrupt the reliability of the communication link. To understand the influence of the channel on the quality of the received signal, it is necessary to model or simulate the optical indoor channel.

A method to simulate the impulse responses for this channel was presented by Barry et al. [3]. Their time-domain approach is based on a microscopic model because it includes all reflections from all surface elements to all others. Higher order reflections caused by multiple rebounds of light from the walls are described by multiple convolutions of the impulse responses. The computation time for this method grows exponentially with increasing order of reflections. In order to save computation time, the approach has been refined and numerically simplified by Carruthers et al. [4], [5] and, using a similar method, by Alqudah and Kavehrad [6]. These two improved methods are physically equivalent to the one described by Barry et al. [3], but they allow the calculation of much higher reflection orders.

Although the above mentioned methods were originally developed for infrared (IR) channels, they can be extended to visible light communication (VLC) channels by the approach described by Lee et al. [7]. Their model takes into account the fact that, in contrast to IR communication, the light of a white photo-diode covers a wide range of wavelengths where the reflectivity cannot be assumed to be constant.

Ray-tracing based on Monte-Carlo simulation is another promising approach to obtain impulse responses for the wireless optical indoor channels [8],

[9], [10]. In contrast to the aforementioned methods, they allow a theoretical error analysis [11].

A macroscopic physical model for the optical indoor channel was presented by Jungnickel et al. [12]. In contrast to the microscopic approaches described above, this model does not attempt to include the details of the room, but uses a few parameters to obtain a rough but simple overall transfer function of the whole room. This model provides a very helpful reference channel for the transfer functions obtained from the microscopic channel. However, it can not reproduce the fine structure of the impulse responses that are obtained from the microscopic models.

In this paper, we present a microscopic frequency-domain method for the simulation of the indoor wireless optical communication channel. Our approach calculates channel transfer functions rather than impulse responses. Although it is physically equivalent to the time-domain simulation method of [3] and [4], the frequency-domain method has the benefit that it replaces convolutions by multiplications. This allows the assembling of all surface-to-surface channels into a matrix, so that higher order reflections can be described by matrix multiplications. Using this method, the infinite sum of all reflections of increasing order can be expressed as a geometric series for matrices (called Neumann series) that can be summed up analytically. Hence, in contrast to the approaches described above, we are now able to formulate a closed expression for the transfer function that includes all reflections orders. The corresponding time-domain impulse responses can be obtained numerically by means of the inverse fast Fourier transform (IFFT).

We point out that our approach is related to a method that is called radiosity in the terminology of computer graphics [13]. However, in computer graphics one is only interested in calculating the illumination of surfaces, and not in the description of the communication channel. In contrast to the radiosity approach, our method calculates the whole channel transfer functions. To our knowledge, this has not been previously described in the literature.

We note that – like in all the approaches cited above – our method does not incorporate linear time dispersion effects due to the channel introduced by the hardware of the transmitter or the receiver. But if necessary, because of the linearity of the systems, the impulse responses of the hardware and of the room channel can simply be combined by convolution.

The remainder of this paper is organised as follows. The incoherent optical channel is characterised in Section II together with a brief overview of the models described in the literature. Our frequency-domain approach is then derived and discussed in Section III. In Section IV, we present numerical results and compare them with previous results from the literature. Finally, in Section V, we draw some conclusions.

II. The Channel Model for Incoherent Wireless Optical Communication

A. Impulse Response and Transfer Function

We consider incoherent optical transmission with intensity modulation and direct detection (IM/DD). Intensity modulation means that the information signal is modulated directly on the time-variant transmitted optical power $x(t)$ which is a real-valued and non-negative baseband signal. The receiver is a photo-diode that generates a photo-current that is proportional to the power $y(t)$ of the impinging light. In a noise-free environment, the optical channel is modelled by a linear time-invariant (LTI) system with a real-valued and non-negative impulse response $h(t) \geq 0$. The received signal is given by

$$y(t) = h(t) * x(t)\,. \tag{1}$$

The Fourier transform $H(f)$ of $h(t)$ is the transfer function of the channel. Denoting the statistical average by $\mathrm{E}\{\cdot\}$, we conclude from Equation (1) that the average optical transmitted and received power

$$\Phi_{\mathsf{Tx}} = \mathrm{E}\{x(t)\} \text{ and } \Phi_{\mathsf{Rx}} = \mathrm{E}\{y(t)\}$$

of the channel are related by

$$\Phi_{\mathsf{Rx}} = H(0)\Phi_{\mathsf{Tx}}\,. \tag{2}$$

Because of the above equation, we can interpret $\eta = H(0)$ as the optical channel gain. The received optical power is proportional to $H(0)$, however, the attenuation of the received electrical power density at frequency f is proportional to $|H(f)|^2$. As a consequence, for wideband optical transmission, the planning of the optical link must not only take into account the received optical power, but also the frequency dependence which is characterised by

the transfer function. The main aim of this paper is to develop methods to evaluate that frequency dependence. Note that the transfer function has the property $H(f) = H^*(-f)$ because $h(t)$ is real. Furthermore, the inequality $|H(f)| \leq H(0)$ holds for all frequencies f. The latter property reflects the low-pass behaviour of the channel.

B. Line-of-Sight and Diffuse Link

The total transfer function

$$H_{\mathsf{total}}(f) = H_{\mathsf{Rx,Tx}}(f) + H_{\mathsf{diff}}(f) \tag{3}$$

for the optical indoor channel consists of two contributions: The line-of-sight (LOS) transfer function $H_{\mathsf{Rx,Tx}}(f)$ between transmitter and receiver, and a diffuse component transfer function $H_{\mathsf{diff}}(f)$. This diffuse component is the superposition of all non-LOS components that are due to one or more reflections at the wall surfaces.

1) LOS Link Between Transmitter and Receiver: For the line-of-sight (LOS) link between the transmitter (Tx) and receiver (Rx), the concept of a generalised Lambertian radiator with attenuation factor

$$\eta_{\mathsf{Rx,Tx}} = v_{\mathsf{Rx,Tx}} \frac{m+1}{2\pi} \cos^m \vartheta_{\mathsf{Rx,Tx}} \frac{A_{\mathsf{Rx}} \cos \psi_{\mathsf{Rx,Tx}}}{d^2_{\mathsf{Rx,Tx}}} \tag{4}$$

is a widely accepted model [14], [2]. In that equation, $d_{\mathsf{Rx,Tx}}$ is the distance between transmitter and receiver, A_{Rx} is the receiver area (which is assumed to be small relative to the distances), $\vartheta_{\mathsf{Rx,Tx}} \leq \pi/2$ is the angle of view (relative to the normal direction) of the receiver position when looking from the transmitter, $\psi_{\mathsf{Rx,Tx}} \leq \pi/2$ is the angle of view of the transmitter position when looking from the receiver. The geometrical arrangement is depicted in Figure 1.

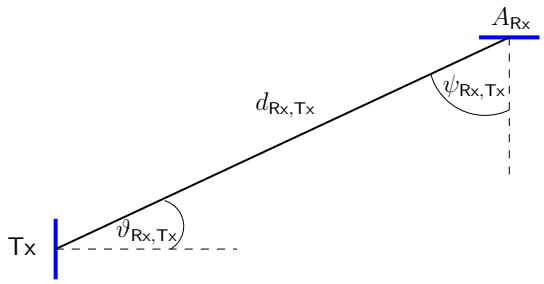

Figure 1. The geometry of transmitter (Tx) and and receiver (Rx).

The transmitter and the receiver are assumed to be hemispherically orientated, which means that $\eta_{\mathsf{Rx,Tx}} = 0$ if one of the angles $\vartheta_{\mathsf{Rx,Tx}}$ or $\psi_{\mathsf{Rx,Tx}}$ exceeds $\pi/2$. This property is included in the visibility factor $v_{\mathsf{Rx,Tx}}$ which is equal to one if the transmitter and the receiver are visible to each other, and it is equal to zero if not. The Lambert index $m \geq 0$ is a measure for the directional characteristics of the transmitter. The special case $m = 1$ corresponds to the (proper) Lambertian radiator which is the common model for a totally diffuse light source. The LOS signal arrives at the receiver with delay $\tau_{\mathsf{Rx,Tx}} = d_{\mathsf{Rx,Tx}}/c$, where c is the speed of light. The LOS link can be alternatively characterised by its impulse response

$$h_{\mathsf{Rx,Tx}}(t) = \eta_{\mathsf{Rx,Tx}}\, \delta(t - \tau_{\mathsf{Rx,Tx}}) \tag{5}$$

or its transfer function

$$H_{\mathsf{Rx,Tx}}(f) = \eta_{\mathsf{Rx,Tx}}\, \mathrm{e}^{-j2\pi f \tau_{\mathsf{Rx,Tx}}}\,. \tag{6}$$

2) Components of the Diffuse Link: The diffuse link is the superposition of all non-LOS links that are due to one or more reflections (bounces) between wall surfaces. We assume purely diffuse Lambertian reflectors which means that specular components are not included in the model. A discrete reflector model is obtained by dividing the walls into small surface elements numbered by $k = 1, ..., N$ with areas A_k and reflectivity factors $\rho_k < 1$. Interpreting each surface element number k as a receiver, the gain factor $\eta_{k,\mathsf{Tx}}$ for the LOS link from the transmitter Tx to surface number k is given by Equation (4), but with the subscript Rx replaced by the index k. The impulse response $h_{k,\mathsf{Tx}}(t)$ and the transfer function $H_{k,\mathsf{Tx}}(t)$ are given by Equations (5) and (6), but also with Rx replaced by k.

Each surface element itself acts as a radiator by reflecting the impinging light, thereby reducing the optical power by the reflectivity factor ρ_k. These surface elements are modelled as proper Lambertian radiators described by Formula (4) with $m = 1$. The gain factor for the LOS link from surface number k to the receiver is thus given by

$$\eta_{\mathsf{Rx},k} = v_{\mathsf{Rx},k} \frac{1}{\pi} \cos \vartheta_{\mathsf{Rx},k} \frac{A_{\mathsf{Rx}} \cos \psi_{\mathsf{Rx},k}}{d^2_{\mathsf{Rx},k}}\,. \tag{7}$$

Similarly, the gain factor η_{ik} for the LOS link from surface number k to surface number i is given by the same equation with Rx replaced by i. Again, the corresponding impulse responses $h_{\mathsf{Rx},k}(t)$ and $h_{ik}(t)$ as well as the transfer functions $H_{\mathsf{Rx},k}(f)$ and $H_{ik}(f)$ are given by Equations (5) and (6), but with

the proper replacements for Rx and Tx. We note that the reflectivity factor ρ_k has not been included in the above definition of gain factors, and thus, must be incorporated separately into the equations for the link budget.

C. Time Domain Simulations of the Diffuse Link

In the time domain simulation approach of Barry et al. [3] which was later improved and refined by Carruthers and Kannan [4], the impulse response $h_{\mathsf{diff}}(t)$ for the diffuse component is approximated by the sum of the contributions from the reflections up to a given order L:

$$h_{\mathsf{diff}}(t) \approx \sum_{\ell=1}^{L} h_{\mathsf{diff}}^{(\ell)}(t) \tag{8}$$

In that equation, the first order term

$$h_{\mathsf{diff}}^{(1)}(t) = \sum_{k=1}^{N} \rho_k h_{\mathsf{Rx},k}(t) * h_{k,\mathsf{Tx}}(t) \tag{9}$$

is the sum of the impulse responses for all paths with exactly one reflection. The second order term

$$h_{\mathsf{diff}}^{(2)}(t) = \sum_{i,k=1}^{N} \rho_i \rho_k h_{\mathsf{Rx},i}(t) * h_{i,k}(t) * h_{k,\mathsf{Tx}}(t) \tag{10}$$

includes all paths with exactly two reflections (one from wall to wall and one from wall to the receiver). The third order term is given by

$$h_{\mathsf{diff}}^{(3)}(t) = \sum_{i,k,l=1}^{N} \rho_i \rho_k \rho_l h_{\mathsf{Rx},i}(t) * h_{i,k}(t) * h_{k,l}(t) * h_{l,\mathsf{Tx}}(t)\,, \tag{11}$$

and so on. In [3] and [4], recursive and iterative formulas for $h_{\mathsf{diff}}^{(\ell)}(t)$ are given. We will relate these formulas to our approach in Subsection III-D.

D. A Heuristic Physical Model for the Diffuse Link

A completely different approach has been proposed by Jungnickel et al. [12]. Their model abstains from a microscopic description of the channel and does not take each single reflection into account. Instead, it considers the channel in total and describes a rough but simple heuristic model with the advantage of a simple analytical formula that fits remarkably well to reality. In this simple model, the channel is the same for all receiver positions and directions. Thus, one would expect that it describes a kind of averaged channel, rather than the fine structure. The model is inspired by the analysis of the integrating sphere, where the channel gain factor and the impulse response can be described by analytical formulas [15]. These formulas are heuristically applied to other geometries by replacing the sphere surface by the surface of the room, A_{room}, and its volume by the volume of the room, V_{room}. The diffuse channel gain factor according to this model is given by

$$\eta_{\mathsf{diff,Jn}} = \frac{A_{\mathsf{Rx}}}{A_{\mathsf{room}}} \frac{\rho}{1-\rho}\,. \tag{12}$$

For a room with constant reflectivity factor ρ, this equation is exactly valid as an average over the whole room. This can be shown by summing up the geometric series

$$\lim_{\ell\to\infty} \sum_{\ell=1}^{L} \rho^{\ell} = \frac{\rho}{1-\rho}\,. \tag{13}$$

For non-constant reflectivity, ρ should be replaced by its average value. As a further refinement, one can replace ρ in the numerator by the reflectivity ρ_1 of the first reflector. The diffuse optical impulse response for a room is modelled as an exponential

$$h_{\mathsf{diff,Jn}}(t) = \frac{\eta_{\mathsf{diff,Jn}}}{\tau} \mathrm{e}^{-t/\tau} \varepsilon(t)\,, \tag{14}$$

where $\varepsilon(t)$ is the unit jump function, and the time constant is given by

$$\tau = -\frac{1}{\ln \rho} \frac{4V_{\mathsf{room}}}{A_{\mathsf{room}} c}\,. \tag{15}$$

The impulse response of Equation (14) corresponds to a first order low-pass filter with transfer function

$$H_{\mathsf{diff,Jn}}(f) = \frac{\eta_{\mathsf{diff,Jn}}}{1 + j2\pi f\tau}\,. \tag{16}$$

III. The Frequency-Domain Simulation Model

In the frequency-domain approach, convolutions can be replaced by multiplications, and higher order reflection terms can simply be expressed by matrix multiplications. As we shall see, this makes it possible to sum up the infinite series for all reflections of any order.

A. Definition of Vector- and Matrix-Valued Transfer Functions

The transfer functions $H_{k,\mathsf{Tx}}(f)$ for the LOS link between transmitter Tx and all the surface elements k of the room are assembled to give the transmitter transfer vector $\mathbf{t}(f)$ defined by

$$\mathbf{t}(f) = \left(\begin{array}{cccc} H_{1,\mathsf{Tx}}(f) & H_{2,\mathsf{Tx}}(f) & \ldots & H_{N,\mathsf{Tx}}(f) \end{array} \right)^{\mathsf{T}} , \tag{17}$$

where $(...)^{\mathsf{T}}$ denotes the transposed vector. We define the frequency-dependent $N \times N$ room-intrinsic transfer matrix $\mathbf{H}(f)$ by its elements

$$[\mathbf{H}(f)]_{ik} = H_{ik}(f) , \tag{18}$$

which are the LOS transfer functions for the link between surface elements k and i. Thus, the matrix $\mathbf{H}(f)$ describes the LOS links between all surfaces inside the room. To include the reflectivity factors ρ_k of the surfaces, we define the $N \times N$ reflectivity matrix

$$\mathbf{G}_\rho = \mathrm{diag}\left(\rho_1, ..., \rho_N\right) . \tag{19}$$

The LOS transfer functions for the link from all the surfaces of the room to the receiver are assembled to give the receiver transfer vector $\mathbf{r}(f)$ which is defined by its transpose

$$\mathbf{r}^{\mathsf{T}}(f) = \left(\begin{array}{cccc} H_{\mathsf{Rx},1}(f) & H_{\mathsf{Rx},2}(f) & \cdots & H_{\mathsf{Rx},N}(f) \end{array} \right) . \tag{20}$$

B. The Neumann Series Approach: Summing up the Contributions for all Bounces

Using these vector and matrix definitions, we obtain more compact expressions for the respective contributions

$$H^{(1)}_{\mathsf{diff}}(f) = \mathbf{r}^{\mathsf{T}}(f)\mathbf{G}_\rho\mathbf{t}(f) , \tag{21}$$

$$H^{(2)}_{\mathsf{diff}}(f) = \mathbf{r}^{\mathsf{T}}(f)\mathbf{G}_\rho\mathbf{H}(f)\mathbf{G}_\rho\mathbf{t}(f) , \tag{22}$$

and

$$H^{(3)}_{\mathsf{diff}}(f) = \mathbf{r}^{\mathsf{T}}(f)\mathbf{G}_\rho\left(\mathbf{H}(f)\mathbf{G}_\rho\right)^2\mathbf{t}(f) \tag{23}$$

to the diffuse transfer function $H_{\mathsf{diff}}(f)$ corresponding to 1, 2, and 3 bounces. These formulas are exact frequency-domain equivalents to Equations (9), (10), and (11). The contribution of reflection order number $\ell = 1, 2, 3, ...$ can more concisely be written as the vector-matrix product

$$H^{(\ell)}_{\mathsf{diff}}(f) = \mathbf{r}^{\mathsf{T}}(f)\mathbf{G}_\rho\left(\mathbf{H}(f)\mathbf{G}_\rho\right)^{\ell-1}\mathbf{t}(f) . \tag{24}$$

The total diffuse transfer function is given by the infinite series

$$H_{\mathsf{diff}}(f) = \sum_{\ell=1}^{\infty} H^{(\ell)}_{\mathsf{diff}}(f) \tag{25}$$

$$= \mathbf{r}^{\mathsf{T}}(f)\mathbf{G}_\rho\sum_{m=0}^{\infty}\left(\mathbf{H}(f)\mathbf{G}_\rho\right)^m\mathbf{t}(f) \tag{26}$$

The Neumann series in this expression can be summed up to

$$\sum_{m=0}^{\infty}\left(\mathbf{H}(f)\mathbf{G}_\rho\right)^m = \left(\mathbf{I} - \mathbf{H}(f)\mathbf{G}_\rho\right)^{-1} , \tag{27}$$

where $\mathbf{I}$ denotes the unity matrix. Inserting Equation (27) into Equation (26) leads to an expression for the diffuse transfer function given by the matrix product

$$H_{\mathsf{diff}}(f) = \mathbf{r}^{\mathsf{T}}(f)\mathbf{G}_\rho\left(\mathbf{I} - \mathbf{H}(f)\mathbf{G}_\rho\right)^{-1}\mathbf{t}(f) . \tag{28}$$

The above formula is the main result of this section. It states that for the diffuse optical channel, the infinite sum for the transfer function of an infinite number of reflections can be calculated by means of elementary matrix operations. It is not necessary to terminate the sum in Equation (25).

C. Formulation as a Recursive LTI System

In the following, we present an alternative recursive derivation of Equation (28) that looks more familiar from the perspective of system theory. Because its physical reasoning is very similar to the radiosity approach in computer graphics [13], this derivation helps us to understand that our method can be interpreted as a generalisation of the radiosity approach.

First we define a length N column vector $\mathbf{s}(f)$ that assembles all transfer functions for all the light (LOS and diffuse) that originally stems from the transmitter and that is impinging on all surface elements indexed by i ($i = 1, ..., N$) . The vector-valued linear time-invariant (LTI) system described by $\mathbf{s}(f)$ is the superposition of two contributions: The first contribution corresponds to all the LOS links directly from the transmitter to all surfaces indexed by i. It is given by the vector-valued transfer function $\mathbf{t}(f)$ defined by Equation (17). The second contribution is the LOS link from all surfaces indexed by k to all surfaces indexed by i, including the reflectivity factor ρ_k. The LOS links between surfaces are described by the elements of the matrix

$\mathbf{H}(f)$ defined by Equation (18). The reflectivities are described by the diagonal matrix $\mathbf{G}_\rho$ defined by Equation (19). Thus, the second contribution is given by $\mathbf{H}(f)\mathbf{G}_\rho\mathbf{s}(f)$. This superposition

$$\mathbf{s}(f) = \mathbf{t}(f) + \mathbf{H}(f)\mathbf{G}_\rho\mathbf{s}(f) \tag{29}$$

can be visualised by the recursive structure depicted in Figure 2. We observe that for the special case $f = 0$, Equation (29) yields the Radiosity Equation (7) in [13] and may thus be interpreted as a generalisation of the Radiosity Equation.

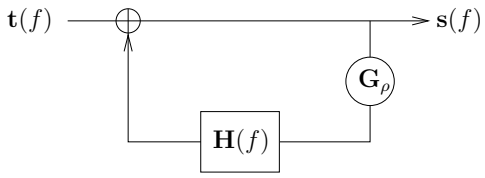

Figure 2. The recursive LTI system for the diffuse light propagation inside the room.

Equation (29) can be solved for $\mathbf{s}(f)$ resulting in

$$\mathbf{s}(f) = \left(\mathbf{I} - \mathbf{H}(f)\mathbf{G}_\rho\right)^{-1}\mathbf{t}(f)\,. \tag{30}$$

The channel given by $\mathbf{s}(f)$ is followed by a second channel that is described by the (length N) row vector $\mathbf{r}^\mathsf{T}(f)\mathbf{G}_\rho$ of all transfer functions for the light impinging at the surface elements indexed by i ($i = 1, ..., N$) and received at Rx. Combining

$$H_{\mathsf{diff}}(f) = \mathbf{r}^\mathsf{T}(f)\mathbf{G}_\rho\mathbf{s}(f)\,. \tag{31}$$

with Equation (30) leads to Equation (28) for the diffuse channel.

D. Relation to the Iterative Time-Domain Approach

We now show how the iterative formula for $h^{(\ell)}_{\mathsf{diff}}(t)$ given in [4] is related to our approach. To do so, we write the diffuse transfer function (24) of order $\ell = 1, 2, 3, ...$ as

$$H^{(\ell)}_{\mathsf{diff}}(f) = \mathbf{r}^\mathsf{T}(f)\mathbf{G}_\rho\mathbf{s}^{(\ell)}(f) \tag{32}$$

with the vector $\mathbf{s}^{(\ell)}(f)$ defined by

$$\mathbf{s}^{(\ell)}(f) = \left(\mathbf{H}(f)\mathbf{G}_\rho\right)^{\ell-1}\mathbf{t}(f)\,. \tag{33}$$

The ith component of this vector, denoted by $H^{(\ell)}_{i,\mathsf{Tx}}(f)$, can be interpreted as the contribution of all ℓth order bounces to the transfer function for the channel from the transmitter to surface element i. Note that

$$H^{(1)}_{i,\mathsf{Tx}}(f) = H_{i,\mathsf{Tx}}(f) \tag{34}$$

is the ith component of vector $\mathbf{t}(f)$ given by Equation (17). The ℓth order transfer function $H^{(\ell)}_{\mathsf{diff}}(f)$ in Equation (32) can thus be interpreted as the succession (as a matrix product) of the ℓth order channel $\mathbf{s}^{(\ell)}(f)$ from the transmitter to all surface elements i and the channel $\mathbf{r}^\mathsf{T}(f)\mathbf{G}_\rho$ from all surface elements i to the receiver. The essential task is the iterative calculation of the channel $\mathbf{s}^{(\ell)}(f)$. To analyse this quantity, we note that Equation (33) for $\ell \geq 2$ can be rewritten as the recursive definition

$$\mathbf{s}^{(\ell)}(f) = \mathbf{H}(f)\mathbf{G}_\rho\mathbf{s}^{(\ell-1)}(f) \text{ with } \mathbf{s}^{(1)}(f) = \mathbf{t}(f)\,. \tag{35}$$

To relate this to the formulation in [4], we must write this vector equation component-wise to obtain the recursion

$$H^{(\ell)}_{i,\mathsf{Tx}}(f) = \sum_{k=1}^{N} H_{ik}(f)\rho_k H^{(\ell-1)}_{k,\mathsf{Tx}}(f) \tag{36}$$

with the start given by Equation (34). We define $\alpha_{ik} = \eta_{ik}\rho_k$ and insert $H_{ik}(f)\rho_k = \alpha_{ik}\mathrm{e}^{-j2\pi f\tau_{ik}}$ into Equation (36) and obtain

$$H^{(\ell)}_{i,\mathsf{Tx}}(f) = \sum_{k=1}^{N} \alpha_{ik}\mathrm{e}^{-j2\pi f\tau_{ik}} H^{(\ell-1)}_{k,\mathsf{Tx}}(f)\,. \tag{37}$$

This means that the ℓth order channel for surface number i is the delayed superposition of all channels of order $\ell - 1$, weighted with attenuation factors α_{ik} that describe the path losses and the reflectivity losses. Transforming Equation (37) to the time domain, we obtain the recursion

$$h^{(\ell)}_{i,\mathsf{Tx}}(t) = \sum_{k=1}^{N} \alpha_{ik} h^{(\ell-1)}_{k,\mathsf{Tx}}(t - \tau_{ik})\,. \tag{38}$$

for the corresponding impulse response $h^{(\ell)}_{i,\mathsf{Tx}}(t)$. This is just the same as Equation (9) in the work of Carruthers and Kannan [4] which corresponds to Equation (13) in the work of Barry et al. [3]. Thus, the time-domain recursion described in [3] and [4] is equivalent to the recursive definition of the ℓth term in the infinite series of Equation (25) in our approach. Their time-domain results for reflections up to order L are equivalent to the restriction of the infinite series of Equation (25) to the finite series

$$H_{\mathsf{diff},L}(f) = \sum_{\ell=1}^{L} H^{(\ell)}_{\mathsf{diff}}(f) \tag{39}$$

in our frequency-domain approach. The frequency-domain approach allows the summing up of the infinite series for the limit $L \to \infty$ analytically without calculating all the ℓth terms explicitly.

E. The Optical Power of the ℓth Bounce

To analyse the optical power transfer, we set $f = 0$ and write $\eta_{i,\mathsf{Tx}}^{(\ell)} = H_{i,\mathsf{Tx}}^{(\ell)}(0)$ for the optical gain factor of the ℓth order channel from the transmitter to surface element number i. By construction, $\eta_{i,\mathsf{Tx}}^{(\ell)}$ is the *received* power gain factor, whereas $\rho_i \eta_{i,\mathsf{Tx}}^{(\ell)}$ is the power gain factor for the light *emitted* from surface number i after ℓ bounces. According to Equation (36), the factor $\eta_{i,\mathsf{Tx}}^{(\ell)}$ fulfils the recursion

$$\eta_{i,\mathsf{Tx}}^{(\ell)} = \sum_{k=1}^{N} \eta_{ik} \rho_k \eta_{k,\mathsf{Tx}}^{(\ell-1)} \,. \tag{40}$$

In this equation, $\eta_{ik} = H_{ik}(0)$ is the optical power gain factor for the LOS link from surface element number k to surface element number i. Assuming that no power is lost in between, the total power originating from element k and arriving at all surface elements i together equals the transmitted power from element k. This fact can be expressed by the equation

$$\sum_{i=1}^{N} \eta_{ik} = 1 \quad \text{for all } k \,. \tag{41}$$

The ℓth order transfer power gain factor from the transmitter to all surface elements is given by the sum

$$\eta_{\mathsf{Tx}}^{(\ell)} \;=\; \sum_{i=1}^{N} \eta_{i,\mathsf{Tx}}^{(\ell)} \,. \tag{42}$$

We insert Equation (40) and obtain

$$\eta_{\mathsf{Tx}}^{(\ell)} = \sum_{i=1}^{N} \sum_{k=1}^{N} \eta_{ik} \rho_k \eta_{k,\mathsf{Tx}}^{(\ell-1)} \,. \tag{43}$$

By interchanging the order of summation and using Equation (41), we get the result

$$\eta_{\mathsf{Tx}}^{(\ell)} = \sum_{k=1}^{N} \rho_k \eta_{k,\mathsf{Tx}}^{(\ell-1)} \,. \tag{44}$$

This equation means that the power transfer from one reflection to the next depends on the illumination of the walls of the preceding reflections. Little power is transferred from bounces $\ell-1$ to ℓ if much optical power is consumed by illuminating the dark parts of the wall at reflection $\ell-1$. Maximal power is transferred if all the optical power is used to illuminate the area where ρ_k is maximal. This intuitively obvious fact follows directly from Equation (44). This is in contradiction to the heuristic assumption that Equation (12) remains valid on average for inhomogeneous reflectivities when replacing ρ by its average value ρ_{ave}. However, for constant reflectivity $\rho_k = \rho$, Equation (44) simplifies to

$$\eta_{\mathsf{Tx}}^{(\ell)} = \rho \eta_{\mathsf{Tx}}^{(\ell-1)} \tag{45}$$

which immediately leads to a geometric series which sums up to Equation (12) with $A_{\mathsf{Rx}} = A_{\mathrm{room}}$. This means that Equation (12) is valid on average at least for receivers at the inner surface of the room. The total diffuse signal power gain for reflections up to order L is then given by

$$\eta_{\mathsf{diff},L} = \sum_{\ell=1}^{L} \rho^{\ell} = \frac{\rho - \rho^{L+1}}{1-\rho} \,. \tag{46}$$

The amount of power that is transmitted by the first L bounces defined by

$$\frac{\eta_{\mathsf{diff},L}}{\eta_{\mathsf{diff},\infty}} = 1 - \rho^{L}$$

is depicted in Figure 3.

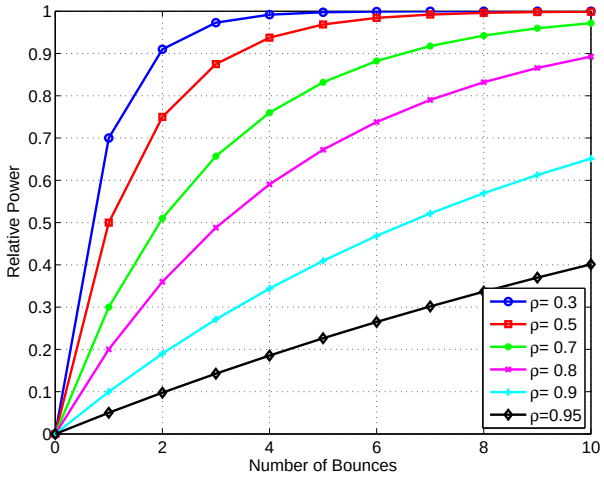

Figure 3. The relative power $\eta_{\mathsf{diff},L}/\eta_{\mathsf{diff},\infty}$ of the diffuse channel for constant reflectivity ρ when L reflections are taken into account.

It shows that for high reflectivity factors ($\rho \gtrsim 0.5$), a significant part ($\gtrsim 10\,\%$) of the total power is transmitted by bounces of order higher than $L = 3$. This underlines the necessity of taking more than a few bounces into account.

F. Calculation of the Impulse Response

The impulse response (diffuse or LOS or the combination of both) $h(t)$ can be obtained from the transfer function $H(f)$ by standard methods applying the inverse fast Fourier transform (IFFT). Let N_{FFT} be the FFT length and Δf the frequency spacing. The transfer function $H(f)$ has to be calculated only for $f = k\Delta f$ with $k = 0, 1, ..., N_{\mathsf{FFT}}/2 - 1$ because $h(t)$ is real and, thus, the negative frequencies can be obtained from $H(-f) = H^*(f)$. We use a raised cosine window for smoothing the signal before applying the IFFT. It must not change the value of $H(0) = \eta$ to retain the correct optical power gain. The time resolution of the calculated impulse response is given by $\Delta t = (N_{\mathsf{FFT}}\Delta f)^{-1}$. If square surfaces A_k with equal edge lengths Δx are used for the tiling of the walls, one should choose $\Delta t \gtrsim \Delta x/c$ in order to avoid discretisation artefacts.

G. Multi-Spot Transmission and Multiple Receiver Positions

In practice, there may be several transmitters, and one is interested in the transfer function for several receiver positions. The extension of the model to multiple-transmitter and multiple-receiver scenarios is straightforward. For K receivers (or receiver positions) with corresponding vectors $\mathbf{r}_k(f)$, $k = 1, ..., K$, we define the matrix

$$\mathbf{R}(f) = \left[\begin{array}{ccc} \mathbf{r}_1(f) & \dots & \mathbf{r}_K(f) \end{array} \right]^{\mathsf{T}} .$$

For L transmitters with corresponding vectors $\mathbf{t}_l(f)$, $l = 1, ..., L$, we define the matrix

$$\mathbf{T}(f) = \left[\begin{array}{ccc} \mathbf{t}_1(f) & \dots & \mathbf{t}_L(f) \end{array} \right] .$$

The transfer function corresponding to the diffuse link from transmitter number l to receiver number k is given the element $[\mathbf{H}_{\mathsf{diff}}(f)]_{kl}$ of the diffuse $K \times L$ transfer matrix

$$\mathbf{H}_{\mathsf{diff}}(f) = \mathbf{R}(f)\mathbf{G}_\rho \left(\mathbf{I} - \mathbf{H}(f)\mathbf{G}_\rho\right)^{-1} \mathbf{T}(f) . \quad (47)$$

The diffuse transfer function $H_{\mathsf{diff},\mathsf{R}\times k}(f)$ for all transmitters at receiver position number k is given at the sum of all elements of row number k for this matrix.

Up to now, all transmitters are assumed to radiate with the same optical power that is normalised to the value 1. To obtain more flexibility in including different values of the transmitter power, we introduce a transmitter gain vector

$$\mathbf{g}_{\mathsf{T}\times} = \left(g_{\mathsf{T}\times 1}, ..., g_{\mathsf{T}\times L}\right)^{\mathsf{T}}$$

and the corresponding transmitter gain matrix

$$\mathbf{G}_{\mathsf{T}\times} = \mathrm{diag}\left(g_{\mathsf{T}\times 1}, ..., g_{\mathsf{T}\times L}\right) . \quad (48)$$

This leads to

$$\mathbf{H}_{\mathsf{diff}}(f) = \mathbf{R}(f)\mathbf{G}_\rho \left(\mathbf{I} - \mathbf{H}(f)\mathbf{G}_\rho\right)^{-1} \mathbf{T}(f)\mathbf{G}_{\mathsf{T}\times} . \quad (49)$$

For all transmitters radiating with the same optical power, we set all entries $g_{\mathsf{T}\times 1}, ..., g_{\mathsf{T}\times L}$ equal to 1. For transmitters radiating with a lower optical power, one may change the corresponding values for $g_{\mathsf{T}\times l}$ ($l = 1, ..., L$). One may, for example, model the switching off of transmitter number l by setting the corresponding value to $g_{\mathsf{T}\times l} = 0$. The complete block diagram for the matrix optical channel is shown in Figure 4.

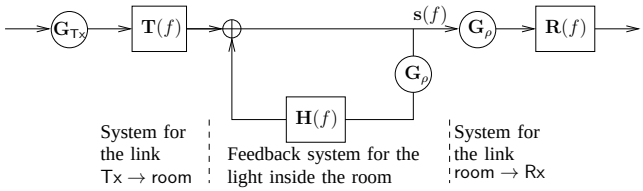

Figure 4. LTI system block diagram for the diffuse optical matrix channel of a room.

We note that in our MATLAB implementation, the computation time hardly changes when the number of transmitters is increased from 1 to 3 and the number of receivers from 1 to 5.

IV. Numerical Results

A. Remarks Concerning the Numerical Complexity

Most of the computational power is needed for the calculation of $\mathbf{s}(f)$ given by Equation (30) for each value of f. Rather than evaluating the expression of type

$$\mathbf{s} = \left(\mathbf{I} - \mathbf{A}\right)^{-1} \mathbf{t} \quad (50)$$

by matrix inversion (here we use the abbreviation $\mathbf{A} = \mathbf{H}(f)\mathbf{G}_\rho$), it is advisable to solve the system of linear equations

$$\left(\mathbf{I} - \mathbf{A}\right) \mathbf{s} = \mathbf{t} \quad (51)$$

for the unknown vector $\mathbf{s}$ by means of standard numerical methods like Gauß elimination. For this

algorithm and an $N \times N$ matrix $\mathbf{A}$, the number of arithmetic operations grows proportional to N^3. This method is feasible for values of N up to the order of a few thousands. For higher values of N, it is recommended to solve the system of linear equations by means of iterative methods [16]. One of these methods is based of the Neumann series which approximates Equation (50) by the finite Neumann series

$$\mathbf{s}_M = \sum_{m=0}^{M} \mathbf{A}^m \, \mathbf{t} \, . \tag{52}$$

This series has the nice physical interpretation that it means that the total diffuse transfer function $H_{\mathsf{diff}}(f)$ is replaced by $H_{\mathsf{diff},L}(f)$ given by Equation (39) which includes only reflections up to order $L = M + 1$. As shown above, Equation (39) is equivalent to the time domain approach described in [3], [4].

The sum in Equation (52) can be computed in a numerically efficient way by means of Jacobi iteration:

$$\mathbf{s}_M = \mathbf{t} + \mathbf{A}\mathbf{s}_{M-1} \text{ with start } \mathbf{s}_0 = \mathbf{t} \, . \tag{53}$$

This iteration replaces the computation of matrix powers $\mathbf{A}^m$ by simple matrix-vector multiplications which reduces the number of arithmetic operations dramatically. The number of operations for each iteration step is proportional to N^2 and, thus, for the whole iteration the total number of operations is proportional to $N^2 \cdot M$. This linear growth in M makes this technique more efficient than the time domain method, because in the original approach [3], the number of arithmetic operations grows exponentially like N^M, and in the improved version described in [4], [5] there remains a growth proportional to $N^2 \cdot M^2$.

When using the finite-order Neumann series method, one needs to know how many reflections L must be considered to obtain results of sufficient accuracy. Depending on the reflectivity factor, the number of necessary iterations may be quite different, see Figure 3. Because this problem does not occur when using the sum formula for $L \to \infty$, one may first estimate a suitable value of L for moderate values of N and then use the Jacobi iteration with this value of L and higher values of N.

B. Comparing with Previous Results

In their pivotal paper [3], Barry et al. present time domain simulations up to reflection order 3 for the indoor channel of four configurations labelled by A, B, C, D. With our frequency domain approach, we are able to reproduce all their finite-order results by evaluating Equation (39). Furthermore, comparing with the numerical results for the infinite sum obtained by evaluating Equation (28), we are able to analyse the residual error due to the termination of the sum.

The residual error is especially significant for configuration A because of its high reflectivity factor $\rho = 0.8$ that is constant for the whole room. Configuration A belongs to a square $5\,\mathrm{m} \times 5\,\mathrm{m} \times 3\,\mathrm{m}$ room of medium office size. The transmitter with $\Phi_{\mathsf{Tx}} = 1\,\mathrm{W}$ and Lambert index $m = 1$ is located at the centre of the ceiling and radiates towards the floor, and the receiver with $A_{\mathsf{Rx}} = 1\mathrm{cm}^2$ is located on the floor facing the ceiling, close to a corner where the LOS light beam is weak. This means that a significant proportion of the received signal is due to the diffused light from the highly reflective walls. The received optical power from the diffuse component versus the maximal included reflection order L is shown in Figure 5. The horizontal lines indicate the asymptotes for $L \to \infty$.

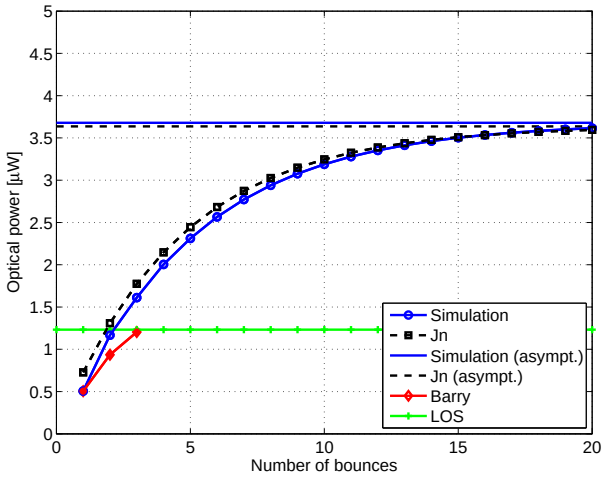

Figure 5. Received optical power (diffuse component) for configuration A versus the order L of reflections (number of bounces) included. Resolution: 8 div/m.

The agreement of our simulations with the curves of Equations (12) and (13) of the Jungnickel (Jn) model is surprisingly good for this configuration. We expect that this is due to the high and constant reflectivity factor ρ and to the proportions of the

room. We have performed some more simulations with the room of configuration A, but with different receiver positions. We find a very good agreement with the Jungnickel model for a receiver on the floor directly facing the ceiling. For a receiver on a wall facing the opposite wall, the agreement is not as satisfactory. Another interesting observation from Figure 5 is that much more than 10 bounces are needed to come close to the true received power. This fact is not surprising, and, as seen in Figure 3, it corresponds to the high reflectivity value $\rho = 0.8$. The values of the *Barry* curve are taken from Figure 3 of Barry et al. [3]. They seem to underestimate the received power even for the first 3 bounces. Up to now, we are not able to explain this deviation that occurs only for configuration A.

The diffuse transfer function for configuration A is shown in Figure 6. The finite order transfer functions according to Equation (39) up to $L = 9$ are drawn as thin solid lines. The infinite sum corresponds to the thick solid line (∞). The dashed line corresponds to the Jungnickel (Jn) model of Equation (16). It turns out that for configuration A, a very high number of bounces is needed to obtain the correct behaviour for low frequencies. Taking only reflections up to order 3 is not enough at low frequencies, but it may be sufficient at high frequencies. At low frequencies $f \lesssim 10\,\mathrm{MHz}$, the Jungnickel (Jn) model according to Equation (16) is very close to our simulation with infinitely many bounces. The total (LOS+diffuse) transfer function

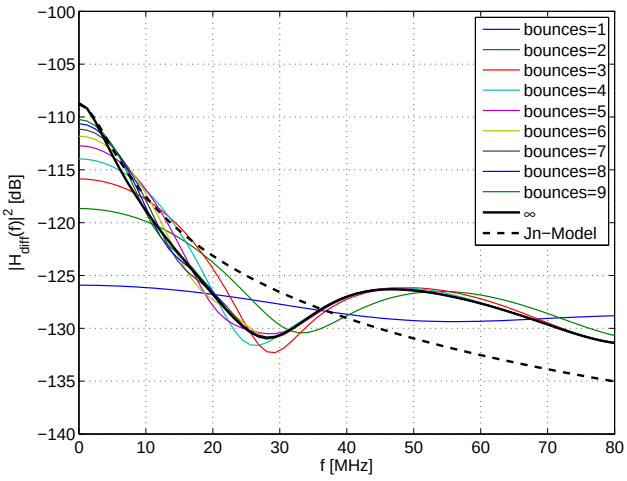

Figure 6. Diffuse transfer function for configuration A. Resolution: 8 div/m.

is depicted in Figure 7 for the same frequency range as in Figure 4 in [3] to allow an easier comparison.

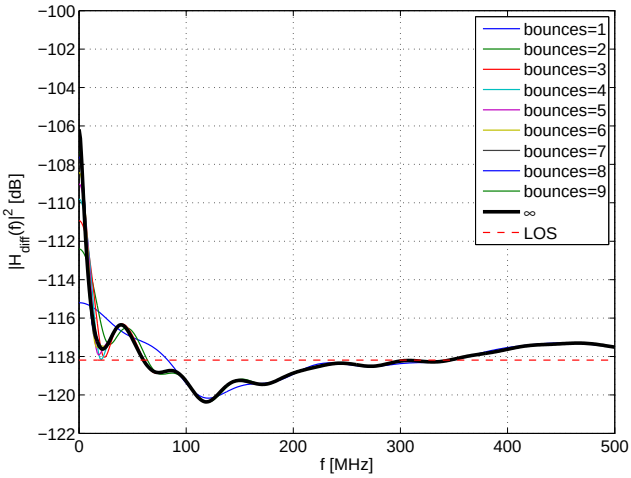

Figure 7. Total (LOS+diffuse) transfer function for configuration A. Resolution: 8 div/m.

The overall agreement is excellent except in the region of very small frequencies, where the deviations take effect which were already discussed by reference to Figure 5.

The impulse response is shown in Figure 8 on a logarithmic scale. The first strong peak corresponds to the LOS signal. The impulse response for an infinite number of reflections shows an exponential decay as predicted by Equation (14) in the Jungnickel model. The figure shows that this exponential decay can hardly be obtained by the first few orders of reflection. Even 9 bounces are not enough to describe this behaviour.

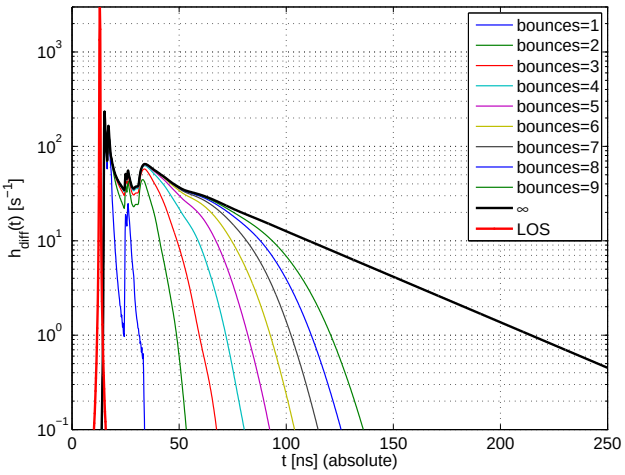

Figure 8. Impulse response for configuration A on a logarithmic scale. Time resolution: 2 ns. Resolution: 8 div/m.

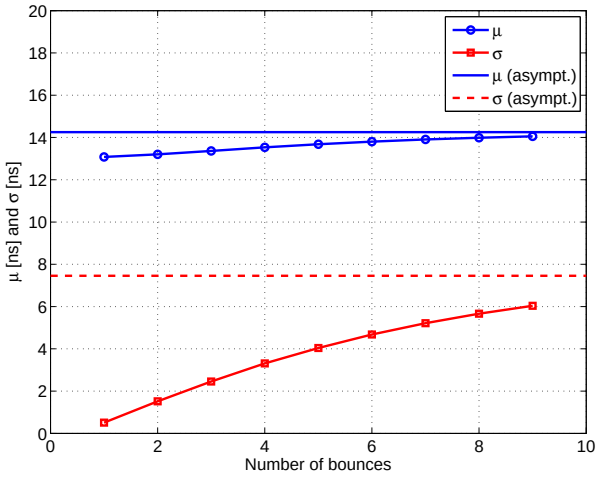

Figure 9. Mean excess delay μ and delay spread σ for configuration A.

The mean excess delay

$$\mu = \frac{\int_{-\infty}^{\infty} t h^2(t)\,\mathrm{d}t}{\int_{-\infty}^{\infty} h^2(t)\,\mathrm{d}t} \tag{54}$$

and the root-mean-square (rms) delay spread

$$\sigma = \sqrt{\frac{\int_{-\infty}^{\infty} (t-\mu)^2 h^2(t)\,\mathrm{d}t}{\int_{-\infty}^{\infty} h^2(t)\,\mathrm{d}t}} \tag{55}$$

are two useful quantities to characterise the time delay and dispersion of an optical channel, respectively [2], [17]. For the method under consideration, μ and σ can be utilised to estimate the accuracy of the finite order approximation in the time-domain. Figure 9 depicts the dependence of both quantities on the maximal included reflection order L for configuration A. The asymptotes for the infinite sum are drawn as horizontal lines. The curve shows that for $L = 3$ with $\sigma^{(3)} = 2.5\,\mathrm{ns}$, the delay spread is underestimated by a factor of 3. For $L = 9$ with $\sigma^{(9)} = 6.0\,\mathrm{ns}$, the delay spread is still underestimated by 20%. We thus conclude that for such high reflectivity factors like $\rho = 0.8$ in this configuration, one must incorporate a higher number of reflection orders into the approximation or better use the formula of the infinite sum.

Configurations B, C, D all belong to the same rectangular $7.5\,\mathrm{m}\times5.5\,\mathrm{m}\times3.5\,\mathrm{m}$ room with different wall reflectivities that are all significantly smaller than for configuration A. The reflectivity of one wall is changed when switching from B to C and D, and the transmitter and receiver locations and directions are changed between the configurations.

For the configurations A, B, C, D, the received optical power values Φ_{Rx}, the mean excess delays μ, and the delay spreads σ are listed in Table I.

Table I
RECEIVED POWER Φ_{Rx}, MEAN EXCESS DELAY μ, AND DELAY SPREAD σ FOR THE BARRY CONFIGURATIONS. THE 3RD ORDER QUANTITIES ARE DENOTED BY $\Phi_{\mathrm{Rx}}^{(3)}$ AND $\sigma^{(3)}$.

	A	B	C	D
Φ_{Rx}	$4.91\,\mu\mathrm{W}$	$0.32\,\mu\mathrm{W}$	$0.31\,\mu\mathrm{W}$	$0.75\,\mu\mathrm{W}$
$\Phi_{\mathrm{Rx}}^{(3)}$	$2.84\,\mu\mathrm{W}$	$0.31\,\mu\mathrm{W}$	$0.29\,\mu\mathrm{W}$	$0.72\,\mu\mathrm{W}$
μ	14.3 ns	17.9 ns	16.5 ns	22.0 ns
σ	7.5 ns	0.9 ns	1.4 ns	2.5 ns
$\sigma^{(3)}$	2.5 ns	0.9 ns	1.3 ns	2.3 ns

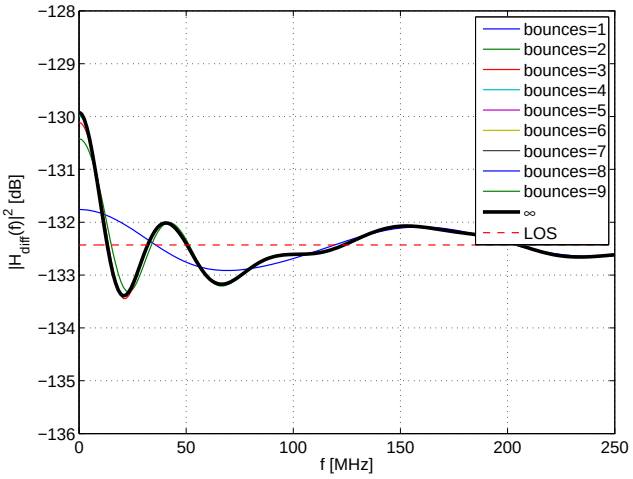

Figure 10. Total (LOS+diffuse) transfer function for configuration B. Resolution: 5 div/m.

The total (LOS+diffuse) transfer function for configuration B depicted in Figure 10 shows excellent agreement with the simulated curve in Figure 6 (c) in [3] for $L = 3$ bounces. The measured curve that is drawn in the same figure in [3] is 2 dB higher near $f = 0$, which is explained by the authors as being due to the small order of the reflection taken into account and by the idealised models for the reflectors. As can be surmised from our simulated curve for infinite order in Figure 10, only a minor part (below 1dB) of the deviation can be explained by the small order of reflection. In contrast to configuration A, the first few orders of reflections are sufficient to reveal the correct behaviour of the transfer function. The value of the total received power of $0.31\,\mu\mathrm{W}$ reported in Table II in [3] for reflections up to order $L = 3$ agrees with our simulation result for $\Phi_{\mathrm{Rx}}^{(3)}$ shown in Table I. For the limit $L \to \infty$, we obtain $\Phi_{\mathrm{Rx}} = 0.32\,\mu\mathrm{W}$.

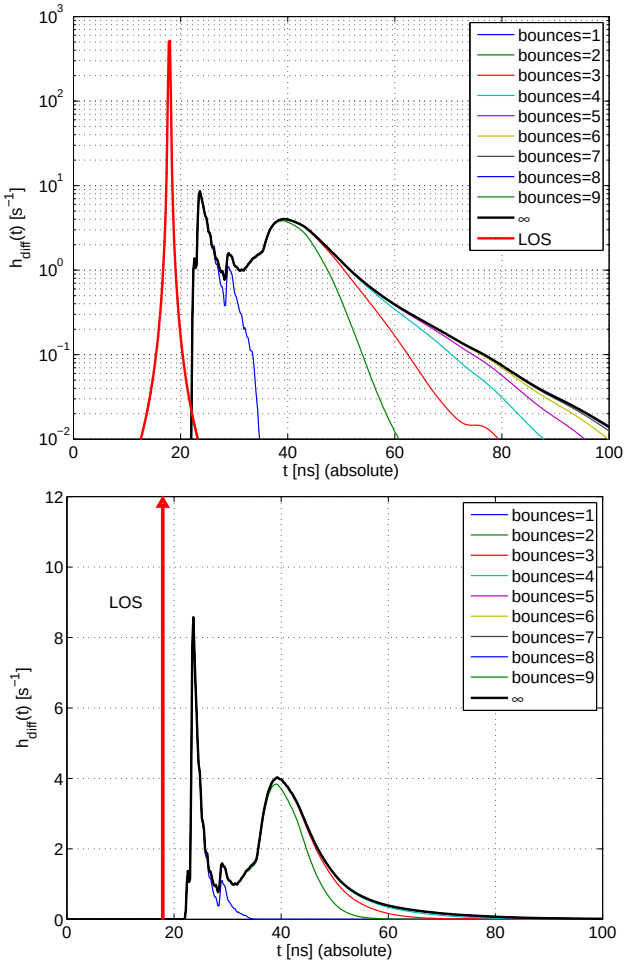

Figure 11. Impulse response for configuration B on a logarithmic (upper plot) and a linear scale (lower plot). Time resolution: 2 ns. Resolution: 5 div/m.

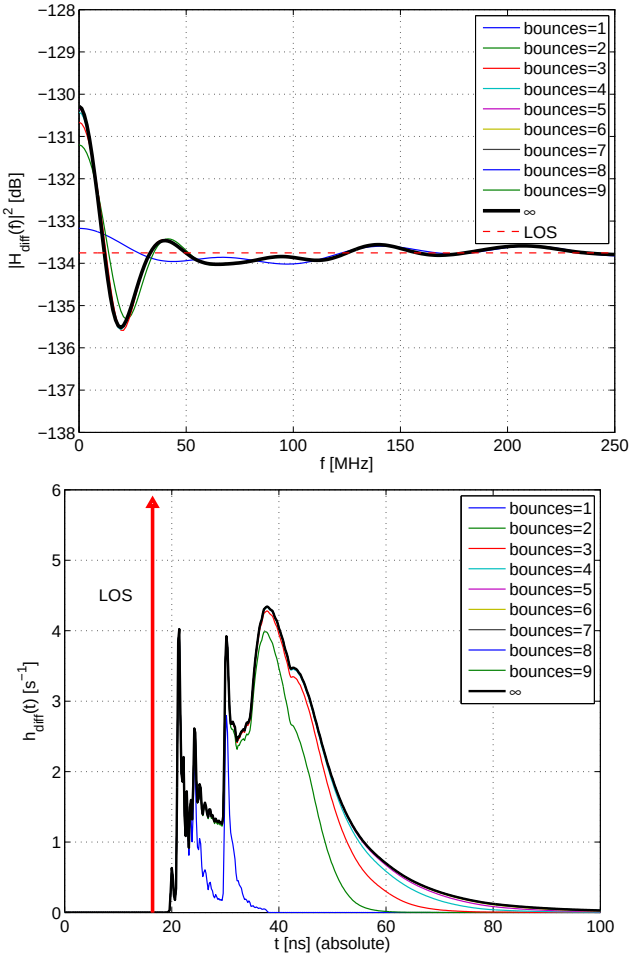

Figure 12. Total (LOS+diffuse) transfer function for configuration C (upper plot) impulse response (lower plot). Time resolution: 2 ns. Resolution: 5 div/m.

The impulse response drawn on a logarithmic scale and on a linear scale is shown in the upper and the lower part, respectively, of Figure 11. The impulse response for an infinite number of reflections shows an exponential decay as predicted by Equation (14) in the Jungnickel model. The correct decay is also achieved for a reflection order higher than $L = 5$. The delay spread $\sigma = 0.9\,\mathrm{ns}$ obtained for an infinite number of reflections is already reached for $L = 3$. The fact that lower reflection orders are sufficient for this configuration is due to lower reflectivity values of the walls.

Configuration C is similar to configuration B, but with higher reflectivity for one wall and slightly different receiver and transmitter positions and directions. Figure 12 shows the total (LOS+diffuse) transfer function in the upper plot and the impulse response (on a linear scale) in the lower plot. For $L = 3$, both show an excellent agreement with Figures 7 (b) and (c) in [3]. As for Configuration B, the measured curve that is drawn in the figure in [3] is 2 dB higher near $f = 0$, and the same explanations are given by the authors. As can be surmised from our simulated curve for infinite order in Figure 12, again only a minor part (below 1dB) of the deviation can be explained by the small order of reflection.

The total received power of $\Phi_{\mathrm{Rx}}^{(3)} = 0.29\,\mu\mathrm{W}$ in Table I obtained from our calculations for reflections up to order $L = 3$ is slightly higher than the value $0.28\,\mu\mathrm{W}$ reported in Table II in [3]. For $L = 6$, the limit for $L \to \infty$ of $\Phi_{\mathrm{Rx}} = 0.31\,\mu\mathrm{W}$ is practically reached. The delay spread $\sigma = 1.4\,\mathrm{ns}$ obtained for an infinite number of reflections is reached for $L = 6$.

For configuration D the wall reflectivities are the same as for configuration C, but the LOS component is absent because the transmitter and receiver are

both facing in the direction of the ceiling. Figure 13 shows the total (LOS+diffuse) transfer function in

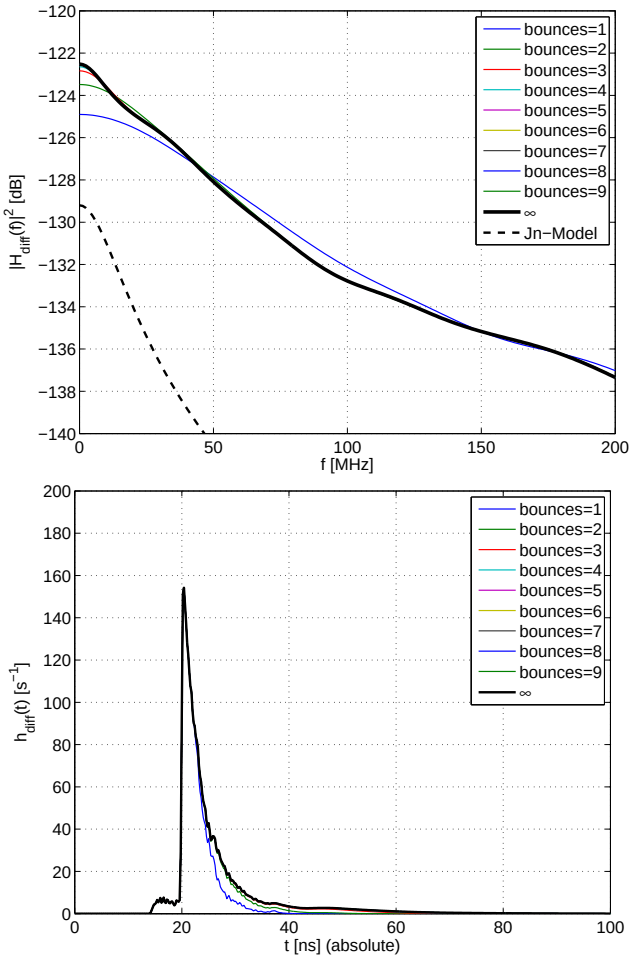

Figure 13. Total (LOS+diffuse) transfer function for configuration D (upper plot) impulse response (lower plot). Time resolution: 2 ns. Resolution: 5 div/m.

the upper plot and the impulse response (on a linear scale) in the lower plot. For $L = 3$, both show an excellent agreement with Figures 8 (b) and (c) in [3]. The agreement with the experimental curve is better than for the other configurations. This topic is discussed in [3] in some detail. It is apparent from the upper plot that the prediction of the Jungnickel model (dashed curve) significantly underestimates the transfer function. One should keep in mind that this model only predicts a rough estimate for a global transfer function for the whole room because it does not incorporate the transmitter and receiver positions and directions. It should be mentioned that for configurations B and C, the Jungnickel model significantly overestimates the transfer function (for sake of clarity, this is not shown in the figures above).

The total received power of of $\Phi_{\mathsf{Rx}}^{(3)} = 0.72\,\mu\mathrm{W}$ in Table I obtained from our calculations for reflections up to order $L = 3$ is slightly higher than the value $0.69\,\mu\mathrm{W}$ reported in Table II in [3]. For the limit $L \to \infty$, we obtain $\Phi_{\mathsf{Rx}} = 0.75\,\mu\mathrm{W}$. This value is reached at reflection order $L = 6$. The delay spread $\sigma = 2.5\,\mathrm{ns}$ obtained for an infinite number of reflections is reached for $L = 6$. The value $\sigma^{(3)} = 2.2\,\mathrm{ns}$ obtained for $L = 3$ reflections yields a rough approximation.

C. Results for a Multiple-Transmitter Indoor Scenario

As an example scenario, let us consider the $12\,\mathrm{m} \times 10\,\mathrm{m} \times 3\,\mathrm{m}$ model seminar room depicted in Figure 14.

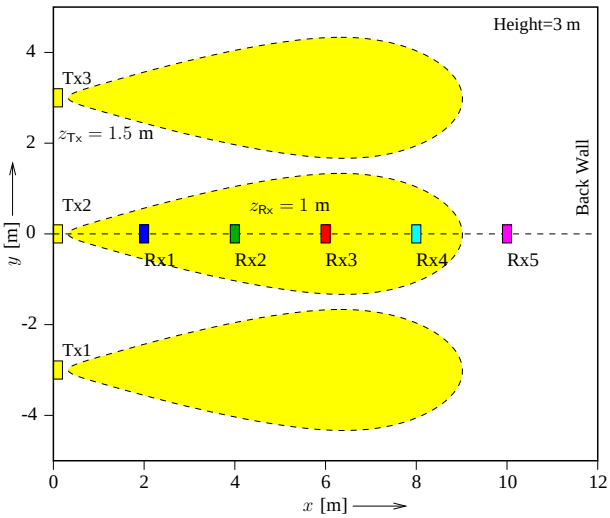

Figure 14. Geometry of the model seminar room with 3 transmitters at the front wall.

The coordinate origin is on the floor at the centre of the front wall. Three transmitters are mounted at the front wall with $x_{\mathsf{Tx}} = 0$ at height $z_{\mathsf{Tx}} = 1.5\,\mathrm{m}$. One is at the centre position with $y_{\mathsf{Tx}} = 0$ and two at the right and left side positions with $y_{\mathsf{Tx}} = \pm 3\,\mathrm{m}$. Each of them radiates with $\Phi_{\mathsf{Tx}} = 1\,\mathrm{W}$, and their light beams point into the y-direction towards the back wall. This is in contrast to the Barry configurations where the transmitters are oriented vertically. The directional characteristics of the transmitters are modelled by a generalised Lambertian radiator with Lambert index $m = 7$. We consider 5 receivers of area $A_{\mathsf{Rx}} = 1\,\mathrm{cm}^2$ positioned at height $z_{\mathsf{Rx}} = 1\,\mathrm{m}$ in the centre of the room at $y_{\mathsf{Rx}} = 0$ with $x_{\mathsf{Rx}} = 2\,\mathrm{m}, 4\,\mathrm{m}, 6\,\mathrm{m}, 8\,\mathrm{m}, 10\,\mathrm{m}$. All

receivers are directed towards the back wall, so that the LOS component is not visible. The reflectivity is assumed to be $\rho = 0.1$ for the floor and $\rho = 0.5$ for all other walls. The transfer functions for the 5 receiver positions are shown in Figure 15.

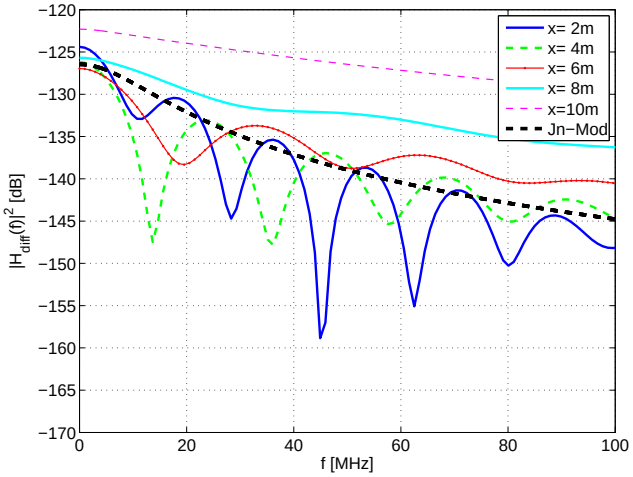

Figure 15. 3 Transmitters: Diffuse transfer functions for 5 receiver positions. Resolution: 3 div/m.

For the first two positions close to the front wall, the channel becomes severely frequency selective and shows distinct notches. These notches are due to the superposition of reflections from the side walls and from the back wall which is directly illuminated and, thus, produces a very strong component with long delay.

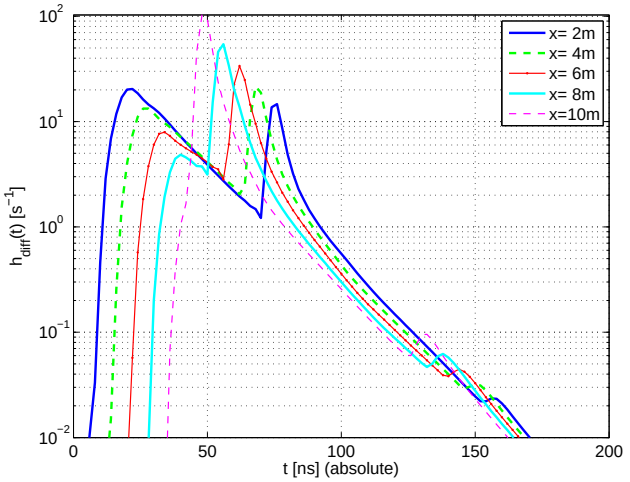

Figure 16. 3 Transmitters: Diffuse impulse response for the receiver looking towards the back wall. Resolution: 3 div/m.

The optical channel gain $\eta_{\text{diff}} = H_{\text{diff}}(0)$ depends on the receiver position. The most distant position receives the strongest signal due to the reflections from the back wall. The received optical power values for the 5 positions are listed in the second row of Table II.

Table II
RECEIVED POWER Φ_{Rx}, MEAN EXCESS DELAY μ, AND DELAY SPREAD σ CORRESPONDING TO FIGURES 15 AND 16.

x	2 m	4 m	6 m	8 m	10 m
Φ_{Rx}	0.60 μW	0.49 μW	0.45 μW	0.52 μW	0.77 μW
μ	34.0 ns	50.0 ns	59.4 ns	56.0 ns	49.2 ns
σ	19.8 ns	19.6 ns	9.4 ns	3.4 ns	2.3 ns

We observe that in Figure 15, the curve of the Jungnickel model is somewhere in the middle between the curves for the different receiver positions. It can therefore be interpreted as a kind of typical transfer function for the room. However, it does not predict any notches. The reasons for the notches become vividly apparent when looking at the impulse responses which are shown in Figure 16. The components due to multiple reflections become clearly visible, and it is possible to relate their run-times to the geometry of the room. The earliest components are due to reflections from the side walls. The significant series of 5 equally spaced peaks starting at $\approx 47\,\text{ns}$ can be identified as the first reflections from the back wall with runlengths $(12 + 2k)\,\text{m} = c \cdot (40 + 6.7k)\,\text{ns}$ for $k = 1, 2, ..., 5$. The weak repetitions of these peaks $80\,\text{ns}$ later are due to 3rd order reflections: Back wall to front wall, front wall to back wall, back wall to receiver. Note that $2 \cdot 12\,\text{m} = c \cdot 80\,\text{ns}$. The exponential decay predicted by the Jungnickel model can be observed as the asymptotic behaviour for long delays. The mean excess delay μ and the delay spread σ are listed in the 3rd and 4th row of Table II. It is interesting to observe that μ decreases for the two most distant positions. This is due to the fact that most of the signal is received through the reflections from the back wall. This has also a strong influence on the delay spread which becomes very small for these positions.

V. CONCLUSION

We have developed a new frequency-domain matrix formalism to describe the wireless optical indoor channel for a room with Lambertian reflectors. This approach leads to a closed expression for the infinite sum of all contributions of arbitrarily high reflection order for the transfer function. The corresponding

impulse responses can be calculated by means of the IFFT. The method can be extended to multi-spot transmission without a significant increase in the computational complexity.

With our frequency-domain method, it is possible to reproduce all the finite-order time-domain results presented by Barry et al. [3] and to compare them with our infinite-order results. Furthermore, we have investigated a model scenario with multiple reflections between back and front walls. In future work, our simulation approach will be extended to include rooms containing obstacles and furniture like it has been done in [4] for the time-domain approach. However, in contrast to painted walls, the surfaces of most kinds of furniture can not appropriately be modelled by purely diffuse Lambertian reflectors. It is thus desirable to extend our model to non-Lambertian reflectors.

REFERENCES

[1] J. R. Barry, *Wirless Infrared Communications*. Kluwer, 1994.
[2] J. M. Kahn and J. R. Barry, "Wireless infrared communications," *Proc. of the IEEE*, vol. 85(2), pp. 265–298, 1997.
[3] J. E. Barry, J. M. Kahn, W. J. Krause, E. A. Lee, and D. G. Messerschmitt, "Simulation of multipath impulse response for indoor wireless optical channels," *IEEE Transactions on Selected Areas in Communications*, vol. 11(3), pp. 367–379, 1993.
[4] J. B. Carruthers and P. Kannan, "Iterative site-based modeling for wireless infrared channels," *IEEE Transactions on Antennas and Propagation*, vol. 50(5), pp. 759–765, May 2002.
[5] J. B. Carruthers, S. M. Carroll, and P. Kannan, "Propagation modelling for indoor optical wireless communications using fast multi-receiver channel estimation," *IEE Proceedings Optoelectronics*, vol. 150(5), pp. 473–481, November 2003.
[6] Y. A. Alqudah and M. Kavehrad, "MIMO characterization of indoor wireless optical link using a diffuse-transmission configuration," *IEEE Transactions on Communications*, vol. 51(9), pp. 1554–1560, September 2003.
[7] K. Lee, H. Park, and J. R. Barry, "Indoor channel characteristics for visible light communications," *IEEE Communications Letters*, vol. 15(2), pp. 217–219, January 2011.
[8] F. J. López-Hernández, R. Pérez-Jiménez, and A. Santamaría, "Ray-tracing algorithms for fast calculation of the channel impulse response on diffuse IR wireless indoor channels," *Optical Engineering*, vol. 39(10)), pp. 296–300, February 2002.
[9] S. Rodríguez Pérez, R. Pérez-Jiménez, F. J. López-Hernández, and A. J. Ayala Alfonso, "Reflection model for calculation of the impulse response on IR-wireless indoor channels using ray-tracing algorithm," *Microwave and Optical Technology Letters*, vol. 32(4), pp. 2775–2780, January 2002.
[10] S. P. Rodríguez, R. Pérez-Jiménez, B. R. Mendoza, F. J. López-Hernández, and A. J. Ayala Alfonso, "Simulation of impulse response for indoor visible light communications using 3D CAD models," *EURASIP Journal on Wireless Communications and Networking*, vol. 2013/1/7, pp. 1–10, 2013, doi:10.1186/1687-1499-2013-7.
[11] O. González, S. P. Rodríguez, R. Pérez-Jiménez, B. R. Mendoza, and A. Ayala, "Error analysis of the simulated impulse response on indoor wireless optical channels using a monte carlo-based ray-tracing algorithm," *IEEE Transactions on Communications*, vol. 53(1), pp. 124–130, January 2005.
[12] V. Jungnickel, V. Pohl, S. Nönnig, and C. von Helmolt, "A physical model of the wireless infrared communication channel," *IEEE J. Sel. Areas on Comm.*, vol. 20(3), pp. 631–640, April 2002.
[13] C. M. Goral, K. E. Torrance, and D. P. Greenburg, "Modeling the interaction of light between diffuse surfaces," *Computer Graphics*, vol. 18,3, pp. 213–222, 1984.
[14] F. R. Gfeller and U. Bapst, "Wireless in-house data communication via diffuse infrared radiation," *Proc. IEEE*, vol. 67 (11), pp. 1474–1486, November 1979.
[15] V. Pohl, V. Jungnickel, and C. von Helmolt, "Integrating-sphere diffusor for wireless infrared communication," *IEE Proc. Optoelectron.*, vol. 147(4), pp. 281–285, August 2000.
[16] G. H. Golub and C. F. Van Loan, *Matrix Computations*, 4th ed. John Hopkins University Press, 2013.
[17] M. R. Pakravan, M. Kavehrad, and H. Hashemi, "Indoor wireless infrared channel characterization by measurements," *IEEE Transactions on Vehicular Technology*, vol. 50(4), pp. 1053–1072, July 2001.